EXPERIMENTAL INVESTIGATION OF FACTORS AFFECTING INDIVIDUAL FIREBRAND HEAT TRANSFER

Amy E. Mensch*, Savannah S. Wessies, Emma M. Veley

National Institute of Standards and Technology, Gaithersburg, MD

ABSTRACT

Firebrand ignition is a significant contributor to the spread of wildfires into communities. This study investigates effects of flow velocity, firebrand wood type and size, and substrate material on the peak heat flux and total heat transfer from individual disc-shaped firebrands. Firebrand heat transfer to a surface is measured with a thin skin calorimeter embedded in the substrate. Peak heat fluxes were between 22 kW/m^2 and 84 kW/m^2 and were higher for the smaller radius firebrands. The total heating to the substrate also tended to be higher for the smaller radius firebrands, but was about the same for the two substrate materials tested. Notably, flow velocity had almost no impact on peak heat flux, and higher velocities increased the total heating only for some firebrand wood types. Two correlations were determined to predict peak heat flux and total heating based on experimental parameters, which included the measured firebrand temperature. These correlations confirmed the importance of substrate properties on firebrand heat transfer.

Keywords: firebrand, heat flux, heat transfer

NOMENCLATURE

A_{surf}	Contact surface area [m^2]
C_p	Specific heat capacity [J kg^{-1} K^{-1}]
k	Thermal Conductivity [W m^{-1} K^{-1}]
m	Initial firebrand mass [kg]
Q	Total heat transfer [MJ m^{-2}]
q	Heat transfer [kW]
q"	Heat flux [kW m^{-2}]
U	Velocity [m s^{-1}]
r	Firebrand radius [m]
T	Temperature [K]
t	Time [s]
t_c	Combustion time [s]

Greek

δ	Thin-skin calorimeter thickness [m]
Π	Non-dimensional group [-]
ρ	Density [kg m^{-3}]

Abbreviations

TC	Thermocouple
TSC	Thin-skin calorimeter

Superscripts and subscripts

cond	Conduction into substrate
FB	Firebrand
net	Net from firebrand
peak	Maximum value
s	Substrate
stor	Stored in TSC

*Corresponding author: amy.mensch@nist.gov

1. INTRODUCTION

The threat of wildland-urban interface (WUI) fires to cause substantial loss of life and property has been growing as a result of increasing fire severity [1] and increasing development in WUI areas [2]. Some of the most deadly and destructive recent fires, such as the 2018 Camp Fire in California and the 2023 Maui Fire, have been driven by high winds and long range spotting [3, 4]. These conditions highlight the importance of firebrands as a significant driver of fire spread and structural ignitions [5]. Firebrands are fragments of burning material that break off from burning vegetation or structures and can be lofted by high winds to deposit far from where they originate. Firebrands pose an ignition threat to structural materials or the surrounding vegetation, whether the firebrands are still flaming or just smoldering when they deposit. Post-fire investigations of WUI fires in Australia [6], the United States [7, 8], and Portugal [9] have reported that firebrands caused or contributed to at least 60 % to 90 % of structural ignitions in those incidents. While multiple firebrands collecting in a pile on a substrate pose a more severe hazard to the substrate, it has also been shown that a single smoldering firebrand can ignite a cellulosic fuel bed [10–13]. Reviews of the current understanding of firebrand ignition mechanisms can be found in Nazare et al. [5], Manzello et al. [14], and Rein [15].

Firebrand ignition is a complex phenomenon determined by the transient heat transfer processes between the firebrands, the substrate and the surroundings. Often ignition of a substrate is characterized by one of three criteria: critical ignition temperature of the substrate, critical heat flux to the substrate, or critical mass loss rate of the substrate, which are the lowest values that lead to ignition for any duration of exposure. The critical criteria are determined experimentally by exposing the substrate to a constant radiant heat flux, with or without a pilot flame, un-

til ignition occurs. Critical heat flux values for wood substrates depend on many factors, including the wood type, grain orientation, and convective flow conditions, as well as if the substrate is considered thermally thin or thermally thick [16, 17]. The mode of heat transfer of the applied heat flux also matters, as exposure to conductive heat sources can initiate smoldering fires with a much lower heat flux than exposure to radiant heat sources [15]. In contrast to the experiments used to determine critical ignition criteria, firebrand heat flux is transient in nature and likely a combination of conduction and radiation, depending on the contact between the firebrands and the surface.

Previous measurements that attempt to quantify the ignition propensity of firebrands have typically focused on time-resolved heat flux from the firebrand or firebrands to the substrate surface, and these studies have reported the peak heat flux and, in some cases, the total heat transfer over time. Many studies have investigated the heat flux of firebrand piles [18–22], and a few studies have considered individual firebrands [18, 23, 24]. While an individual firebrand is less likely to ignite a substrate compared to a firebrand pile, heat transfer measurements for a single firebrand have allowed for the development of heat flux measurement techniques and for a more fundamental understanding of the variables and conditions that lead to firebrand ignition. Previous investigations have varied in the firebrand wood types and geometries that have been studied, including Scottish softwood pellets [20], birch cylinders [18, 19, 25], birch discs [19, 24], eucalyptus sticks [19], pine cylinders [26], pine bark [19], and oak cuboids and cylinders [23]. Typically the firebrands are deposited in a smoldering state and exposed to flow velocities up to 2 m/s to represent the low velocities expected to allow firebrand accumulation close to the surface [27]. A few studies of firebrand ignition of substrates have exposed firebrand piles to velocities up to 2.7 m/s [25, 26].

Among previous studies of individual firebrands, the range of peak net heat fluxes have been between 10 kW/m^2 and 50 kW/m^2 (over the firebrand initial projected area), and the range of total heating has been up to 1.6 MJ/m^2 [18, 23, 28] across different firebrand geometries and dimensions, and different measurement methods. Hakes et al. [18] measured the heat flux from individual cylindrical birch firebrands as well as piles using a water-cooled heat flux gauge, and varied the cylinder diameter and flow velocity. The heat flux gauge measurements for individual firebrands were all less than 20 kW/m^2. Bearinger et al. [23] and Wong et al. [28] measured the heat flux from different geometries of individual oak firebrands using inverse heat transfer and infrared thermography on the underside of the substrate. The peak heat fluxes, averaged over the initial firebrand projected area were all less than 30 kW/m^2. They did find peak local heat fluxes (0.4 mm resolution) as high as 105.8 kW/m^2. Mensch et al. [24] measured the heat flux from individual birch disc-shaped firebrands using a thin-skin calorimeter (TSC), and reported a peak net heat flux of 45 kW/m^2 on average. These values were higher than previously measured using other techniques, which may have interfered with the measurement by cooling the firebrand.

None of the previous firebrand heat flux studies found significant differences in peak net heat flux due to the variations in the flow velocity, firebrand geometry or orientation. However, Mensch et al. [24] found that the total heating and duration of heating for the birch disc-shaped firebrands did increase with flow velocity. Bearinger et al. [29] measured heat transfer from firebrand piles and concluded that wind speed, firebrand length, and firebrand aspect ratio were all statistically significant factors affecting the peak heat flux from piles. The current study expands the scope of parameters tested for individual firebrands to analyze the effects of diameter, wood type, external flow velocity, and substrate material on the peak heat flux and total heat transfer to a substrate. The effect of substrate material, in particular, on firebrand heat transfer has not previously been examined in the literature to our knowledge.

2. METHODS

The method of using a size-matched TSC embedded in a substrate to address the heat transfer effects of various properties was previously describe by the authors [24]. Measurements of the heat transfer from a deposited firebrand to a substrate were conducted in a single-pass wind tunnel shown in Fig. 1, which exposed the firebrands to steady flow velocities between 0.05 m/s and 2.0 m/s, which are representative of velocities close to the ground in WUI environments and under the estimated critical velocity for firebrands to accumulate, 2.3 m/s [27]. The wind tunnel pulled ambient room air through the flow inlet and a honeycomb flow straightener, and then the flow developed in the main section with a 305 mm by 305 mm cross section for 1.3 m before the firebrand location in the test section. Before each experiment the flow velocities were measured with a PCE-423 hot wire anemometer at the location of the firebrand, 12.7 mm above the surface. The anemometer used sampled the flow at a rate of 1.25 Hz, with a resolution of 0.01 m/s and an accuracy of 0.25 m/s. The standard uncertainty for the repeated velocity measurements at that location was about 6 % for all flow conditions.

Glowing firebrands were generated from wood discs cut from birch, pine, cedar, and oak dowels. These wood types were used in other studies [18, 19, 23, 24, 28] and were commercially available. There were two sizes of wood discs tested, both with the same thickness to diameter ratio, 1:3. The larger discs had a thickness of 10.6 mm ± 0.2 mm and a diameter of 31.6 mm ± 0.2 mm. The smaller discs had a thickness of 8.5 mm ± 0.2 mm and a diameter of 25.0 mm ± 0.3 mm. The wood discs were completely dried in an oven at 383 K ± 10 K, as confirmed by successive mass measurements with less than 0.5 % change, before testing. Each wood disc was ignited by placing it under direct flame contact from a propane burner while sitting on the wire mesh base of a metal chimney. The wood was exposed to direct flame contact for approximately 10 s, when it began to burn with a self-sustaining flame. The flaming wood disc burned in the chimney until it self-extinguished, then it was picked up with tongs and placed on the substrate through the side door of the wind tunnel shown in Fig. 1. The firebrand continued to smolder and often was visibly glowing in the wind tunnel during the test. This firebrand generation procedure was demonstrated to be repeatable because the time until self-extinguishment and the internal wood temperature was found to be consistent for the same wood type and size of disc [24].

Once deposited, the firebrand was observed from above by a digital camera in the visible range, and in a few experiments, an infrared camera was also used to record the firebrand temper-

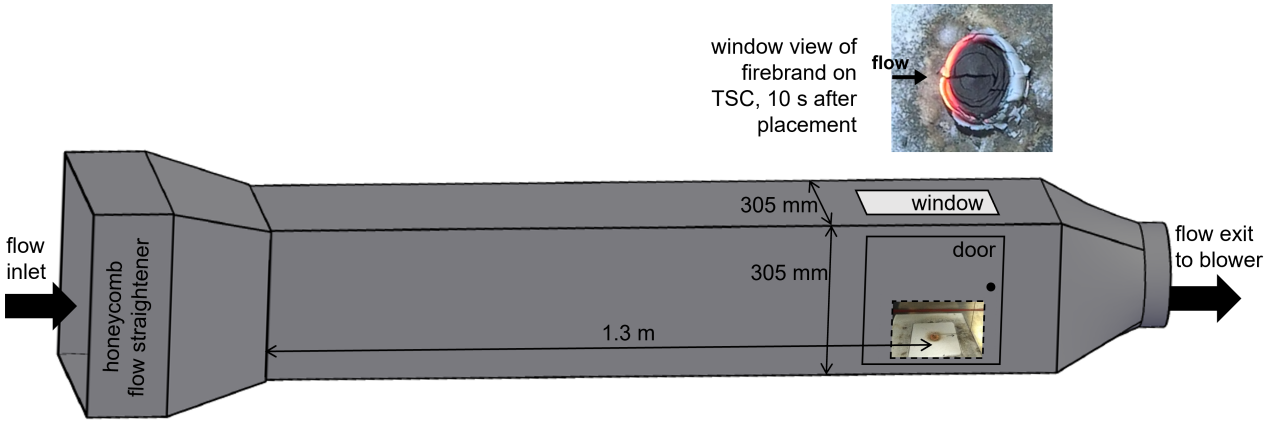

FIGURE 1: DEPICTION OF THE SINGLE-PASS WIND TUNNEL TO GENERATE FLOW VELOCITIES BETWEEN 0.05 m/s AND 2 m/s. THE TSC AND SUBSTRATE ARE SHOWN BEHIND THE SIDE DOOR.

atures. The cameras were mounted to view the firebrand through the window shown in Fig. 1. A circular hole was cut in the window for the infrared camera, a FLIR T560[1], which recorded infrared data at a rate of 30 frames/s at a resolution of 640 x 480 pixels. The temperatures were calculated using an emissivity for the firebrand of 0.8, as measured in Wessies et al. [12], and then the temperatures were averaged over the firebrand top surface area and averaged for the first 5 s after deposition.

The heat transfer from the firebrand to the substrate was measured using a TSC in the substrate within the wind tunnel. The substrate was approximately 25.4 mm thick, and the material was either ceramic fiber board or silicone. Ceramic fiber board was chosen to represent a highly insulating material, while silicone was chosen because it is a non-flammable material with an order of magnitude larger thermal conductivity as shown in Table 1. The thermal conductivities of these two materials cover a range that is relevant for many wood materials [30] which are commonly used for residential decks and fences. The TSC was constructed in-house out of a thin copper disc, with a thickness, δ, of 0.552 mm ± 0.06 mm, and 0.25 mm K-type thermocouple wires welded to the back surface, and additional K-type thermocouples installed at specific locations within the substrate. The TSC was embedded so that the top surface was flush with the top of the substrate. The TSC diameter was designed to be the same as the approximate size of the firebrand after the generation procedure, which caused the firebrand to shrink. Matching the size of the TSC and the firebrand reduces the error from convection on uncovered TSC surfaces which was mentioned by Hakes et al. [18] as their reason not to use TSCs for their firebrand piles under wind conditions. There were two diameters of the TSC, 25.4 mm and 19.1 mm. Small holes, 1.5 mm and 2.4 mm wide, were drilled for the thermocouple wires to exit through the bottom of the substrate. The values used for the thermophysical properties (thermal conductivity, k, the density, ρ, and the specific heat capacity, C_p) of both substrate materials and the TSC material are given in Table 1.

[1]The instrument is identified in order to specify the experimental procedure adequately. Such identification is not intended to imply recommendation or endorsement of any product or service by NIST, nor is it intended to imply that the instrument is necessarily the best available for the purpose.

TABLE 1: THERMAL PROPERTIES OF THE SUBSTRATE AND TSC MATERIALS

	Substrates		TSC
Material	ceramic fiber board	silicone	copper
k (W/m K)	0.065	0.229	392
ρ (kg/m^3)	336	1049	8960
C_p (kJ/kg K)	1.089	1.175	0.385

The basis of the heat flux measurement was an energy balance on the TSC as shown in Figure 2a. The net heat transfer from the firebrand into the TSC, q_{net}, is equal to the sum of the heat stored in the TSC, q_{stor}, and the conduction losses into the substrate, q_{cond}. Heat losses from the top surface of the TSC are neglected because the bottom of the firebrand has about the same area as the top of the TSC as shown in Figure 2b. The net heat flux from the firebrand, q''_{net}, is determined by dividing q_{net} by the surface area of the TSC exposed to the firebrand, A_{surf}, as shown in Eq. 1.

$$q''_{net} = \frac{q_{stor} + q_{cond}}{A_{surf}} = (\rho C_p \delta)_{TSC} \frac{dT_{TSC}}{dt} + q''_{cond} \quad (1)$$

The lumped capacitance assumption of uniform temperature is applied to the TSC, since its Biot number is estimated to be on the order of 10^{-6} [24] using δ for the characteristic length and a heat transfer coefficient of 1.4 kW/m^{2}K. Therefore, q_{stor}

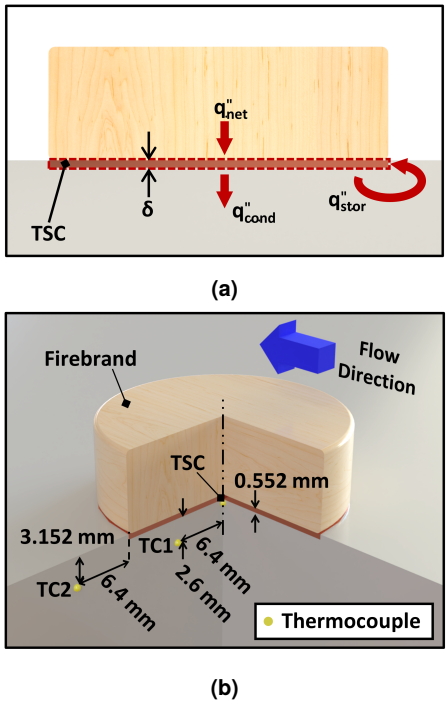

FIGURE 2: DIAGRAMS OF (A) THE TSC SYSTEM AND THERMOCOUPLE (TC) LOCATIONS AND (B) THE THERMAL ENERGY BALANCE ON THE TSC.

is calculated from the rate of change in the temperature of the copper disc [31, 32], which was recorded at a rate of 6 Hz. The response time of the TSC, as defined in ASTM E459 [31], is estimated to be about 0.04 s, which is less than 25 % of the time between successive measurements. The time derivative was computed using a second order central difference of the recorded temperature measurements. Although any effect of the copper TSC on the measurement of firebrand heat flux is expected to be minimal due to its low Biot number and quick response time, one possible verification that the presence of the TSC does not affect the smoldering combustion of the firebrand is to compare the firebrand temperatures measured by IR imaging. Additional tests were conducted where the firebrands were placed directly on the substrate material, and the IR firebrand temperatures in the first 5 s after placement were within 5 % of the average IR firebrand temperatures measured when a TSC was present. The glowing times (duration that glowing was observed from the top of the firebrand) without a TSC were also within the range of glowing times recorded for the same conditions with a TSC , supporting the assumption that the TSC is minimally invasive to the firebrand heat flux.

The q_{cond} term was a sum of the vertical and lateral components of conduction losses computed from Fourier's Law using thermocouple measurements within the substrate. These beaded thermocouples were constructed from 0.25 mm K-type wire and are TC1 and TC2 as labeled in Figure 2b. The substrate temperatures were recorded at 3 Hz since they changed more slowly than the TSC temperature. The vertical component of q_{cond} was computed using the temperature difference between the TSC and TC1, and a distance of 2.6 mm. In addition to assuming a uniform temperature for the TSC, it was assumed the substrate temperature 2.6 mm below the TSC aligned with the edge of the TSC was the same as TC1. Therefore, the lateral component of q_{cond} was computed using temperature difference between TC1 and TC2, and the offset distance of 6.4 mm.

As documented in Mensch et al. [24], the general behavior of q''_{net} for individual firebrands was an initial rapid rise, with a peak between 1 s to 3 s after the firebrand was placed on the TSC, followed by a slow decay. Example heat flux profiles for a birch firebrand at the 1 m/s flow condition are given in Figure 3 for both substrates. The initial peak was dominated by the q_{stor} component, while the q_{cond} increased more slowly. The two terms that contribute to q''_{net}, q_{stor}, and q_{cond}, were about the same order of magnitude at around 30 s for the ceramic fiber board substrate in Figure 3a and before 10 s for the silicone substrate in Figure 3b. Then q_{stor} continued to decrease, while q_{cond} tended to reach a relatively steady value. The 95 % confidence-level combined measurement uncertainty in the peak q''_{net} measurement was ± 17 % on average, with the largest contribution from the numerical calculation of dT_{TSC}/dt. A description of the peak q''_{net} uncertainty estimation was detailed in Mensch et al. [24].

The total heating of the substrate due to the firebrand, Q, was calculated by integrating q''_{net} from the time of deposition until the time when q''_{net} had dropped to 2 kW/m^2. The end time for the integration to calculate Q is shown in Figure 3 with an x, and this duration is hereafter referred to as the combustion time. The 95 % confidence-level combined measurement uncertainty in Q was ± 8 % on average, calculated by propagating the uncertainty in q''_{net} through the numerical integration.

3. RESULTS

Over the course of these experiments, 150 firebrand heat flux profiles, such as those in Figure 3, were measured, spanning four wood types, two firebrand sizes, two substrate materials, and four flow conditions. Figure 4 shows images from the visible spectrum camera of the four small firebrand wood types at 30 s and 180 s after deposition for the 1 m/s flow condition on both the ceramic fiber board and silicone substrates. At 30 s, all of the firebrands except oak on the silicone substrate (Figure 4h) were still glowing along the leading edge. At 180 s, none of the firebrands were still glowing; however, ash had formed on all the firebrands, with the oak firebrands having significantly less than the others. While the firebrands may no longer be glowing at 180 s, many were still heating the substrate with a heat flux greater than 2 kW/m^2. The combustion times for pine and birch were longer than 180 s regardless of substrate type or flow rate. The average combustion times from deposition to 2 kW/m^2 are listed in Table 2 along with the 95 % confidence in the mean value for at least three repeat tests.

The peak q''_{net} occurred within the first few seconds after deposition onto the TSC and was mostly dependent upon the q''_{stor} as was shown in Figure 3. Although the peak q''_{net} for the case in Figure 3 was much higher for ceramic fiber board substrate than for the silicone substrate, Q was similar for both materials. The peak q''_{net} measurements, which will hereafter be referred to as $q''_{net,peak}$, for the small firebrands are presented for both substrate types in Figure 5, where the symbols show values from individual

TABLE 2: SUMMARY OF THE COMBUSTION TIMES FOR ALL FIREBRAND TYPES UNDER ALL FLOW CONDITIONS ALONG WITH THE 95 % CONFIDENCE IN THE MEAN VALUE FOR REPEAT TESTS

Substrate	Firebrand Size	Flow (m/s)	Pine (s)	Birch (s)	Cedar (s)	Oak (s)
ceramic fiber board	small	0.05	325 ± 26	399 ± 97	93 ± 5	92 ± 11
		0.6	326 ± 34	400 ± 78	87 ± 9	111 ± 69
		1.0	362 ± 21	371 ± 48	96 ± 33	110 ± 69
		1.6	308 ± 52	336 ± 25	136 ± 76	182 ± 103
	large	0.05	573 ± 61	504 ± 77	—	—
		0.6	600 ± 153	364 ± 60	—	—
		1.0	573 ± 128	430 ± 93	—	—
		1.6	607 ± 88	552 ± 284	—	—
silicone	small	0.1	413 ± 72	433 ± 233	117 ± 47	171 ± 21
		0.6	390 ± 61	399 ± 125	127 ± 35	161 ± 19
		1.0	380 ± 57	375 ± 63	121 ± 50	182 ± 42
		1.8	394 ± 17	412 ± 104	177 ± 52	192 ± 30

experiments, and the lines show the mean $q''_{net,peak}$ trend with flow condition. Error bars show the measurement uncertainty at 95 % confidence for the experiment with the greatest uncertainty at each flow condition and wood type. On the ceramic fiber board, $q''_{net,peak}$ ranged from 35 kW/m^2 (oak) to 84 kW/m^2 (birch) as shown in Figure 5a. Oak had the lowest $q''_{net,peak}$ on average, and birch had the highest $q''_{net,peak}$ across all flow velocities. The silicone substrate in Figure 5b has $q''_{net,peak}$ ranging from 22 kW/m^2 (cedar) to 62 kW/m^2 (birch), which was a narrower range than for the peaks seen on the ceramic fiber board substrate. The $q''_{net,peak}$ measured on a silicone substrate generally had a lower magnitude, although the spread of the data overlaps with that from ceramic fiberboard in some cases.

Along with the thermal properties of the substrate, the peak heat flux is also affected by the wood type through the heat generation of the firebrand combustion. The average top surface temperature of the firebrands immediately after deposition is presented as a proxy for the heat generation. Table 3 enumerates the range of average firebrand temperatures obtained from the infrared camera as a function of flow condition and wood type. Across all wood types, the lowest average temperature was measured for the smallest flow velocity, and the firebrand temperatures generally increased with as the flow velocity increased. Cedar had the greatest range in firebrand temperature, and oak had the smallest range and overall lowest temperature. Note that for the pine firebrands, the temperatures in Table 3 are in a reasonable range to that reported for piles of cylindrical pine firebrands measured by color ratio pyrometry [26] considering the size and geometrical differences between the firebrands in that study and this study.

Although firebrand temperatures for most wood types increased with flow velocity, the flow velocity did not appear to have a clear or consistent effect on the peak heat flux, as observed for the various wood type or substrate cases in Figure 5. This differs from many experimental studies of firebrand piles showing increases with flow velocity. However, studies measuring

TABLE 3: AVERAGE FIREBRAND TEMPERATURES (K) FROM IR IMAGING OVER THE FIRST 5 s.

	Flow Condition (m/s)			
Wood	0.05	0.6	1.0	1.6
Pine	889	953	942	996
Birch	870	936	919	934
Cedar	873	924	896	1011
Oak	756	747	750	763

individual firebrand heat flux, such as Bearinger et al. [23], also measured area-averaged heat fluxes with no significant dependence on flow velocity, although localized peak heat fluxes did increase with flow velocity.

The total heating, Q, was q''_{net} integrated over the combustion time, and therefore Q was impacted by both q''_{stor} and q''_{cond}. The Q results for the small firebrands are shown for both substrates in Figure 6, where the symbols show individual experiments, and the lines show the mean Q trend with flow condition. Error bars show measurement uncertainty at 95 % confidence for representative experiments, and in Figure 6a the error bars are smaller than the symbols. Q on the ceramic fiber board (Figure 6a) ranged from 0.54 MJ/m^2 (cedar) to 2.56 MJ/m^2 (birch). Q on the silicone substrate (Figure 6b) had a slightly greater range from 0.30 MJ/m^2 (cedar) to 3.33 MJ/m^2 (birch). Cedar and oak had much lower Q than pine or birch, which had significantly longer combustion times (Table 2) compared to cedar and oak.

The effect of the firebrand radius was tested for two different firebrand sizes using birch and pine on the ceramic fiber board substrate. The large radius (12.7 mm) and the small radius (9.5 mm) were tested across the range of velocities. Figure 7a shows representative q''_{net} profiles for birch for the first 10 s after deposition at the 0.1 m/s flow condition in orange and the 1 m/s flow condition in purple for both the small (thin lines) and large (thick lines) firebrands. Figure 7b similarly shows representative

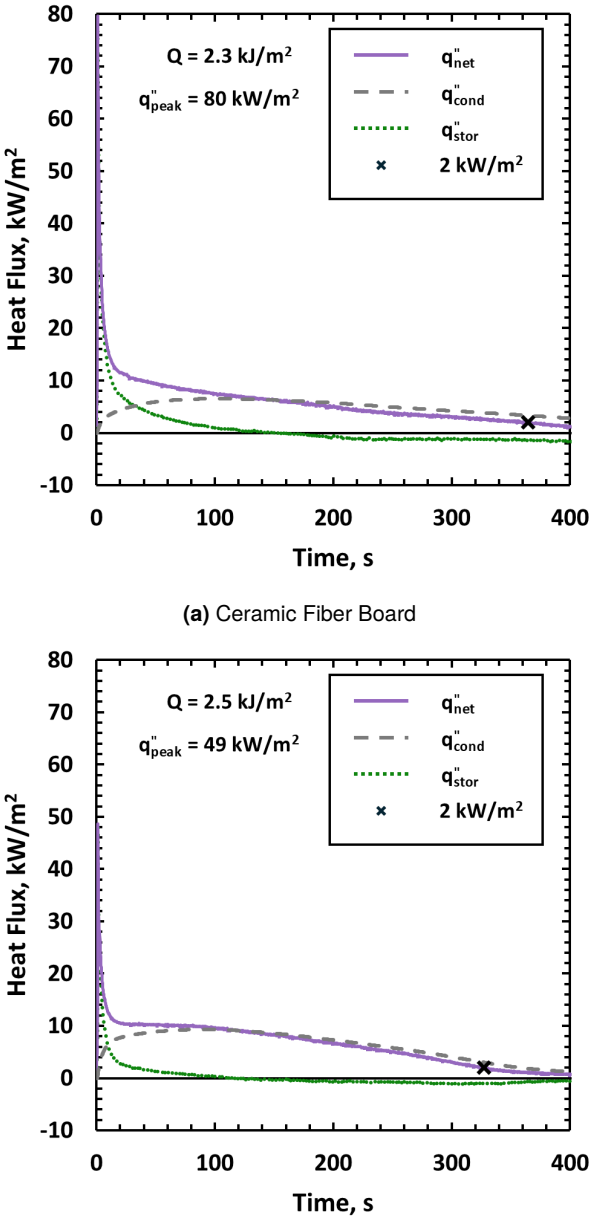

(a) Ceramic Fiber Board

(b) Silicone

FIGURE 3: HEAT FLUX PROFILES FOR BIRCH FIREBRANDS AT THE 1 m/s FLOW CONDITION (A) ON A CERAMIC FIBER BOARD SUBSTRATE AND (B) ON A SILICONE SUBSTRATE.

pine q''_{net} profiles. The profiles in Figure 7 show that the peak q''_{net} for the larger firebrands was lower and slightly delayed from the smaller firebrands, and there was little effect of the flow velocity. The $q''_{net,peak}$ values from the large and small firebrands are shown in Figure 8a where the symbols show individual experiments, and the lines show the averages for each flow condition. Error bars show measurement uncertainty at 95 % confidence for representative experiments. Figure 8a also indicates that the small firebrands had a higher $q''_{net,peak}$ than the corresponding large firebrands. While the small firebrands had higher $q''_{net,peak}$, the small firebrand combustion times, as shown in Table 2, tended to be shorter, especially for pine. However, the average Q for the small firebrands was still higher than the large firebrands for all cases except for pine at the highest flow velocity, as presented in Figure 8b.

4. DIMENSIONAL ANALYSIS

The parameters that were varied in the experiments (wood type, firebrand size, substrate material, and flow condition) were represented by the quantitative values of initial firebrand mass, firebrand radius at deposition, initial firebrand temperature, firebrand combustion time, thermal properties of the substrate material, and air flow velocity. Dimensional analysis was performed on the results to elucidate the relative importance of the different parameters on $q''_{net,peak}$ and Q. The parameters we considered are listed below in Eq. 2 for $q''_{net,peak}$ and Eq. 3 for Q. For the firebrand properties, the parameters were the mass, m, the radius of the firebrand, r, and the firebrand temperature, T_{FB}. An additional firebrand property – the combustion time, t_c – was included in Eq. 3. The m for each firebrand was measured and recorded prior to exposure to the propane burner. The firebrand r was either 12.7 mm or 9.5 mm, estimated from the dimensions at the time of deposition. The T_{FB} and t_c were measured parameters dependent on the wood type and the flow condition (see average values in Table 3 and Table 2). For the substrate material, the parameters considered were the thermal conductivity, k_s, the density, ρ_s, and the specific heat capacity, $C_{p,s}$. The values for the two substrate materials are listed in Table 1. The flow velocity was denoted as U in the dimensional analysis. For the Q analysis, the measured $q''_{net,peak,meas}$ was included as an additional parameter.

$$q''_{net,peak} = f(m,\ r,\ T_{FB},\ k_s,\ \rho_s,\ C_{p,s},\ U) \tag{2}$$

$$Q = f(m,\ r,\ T_{FB},\ t_c,\ k_s,\ \rho_s,\ C_{p,s},\ U,\ q''_{net,peak,meas}) \tag{3}$$

In the two equations above, there were four fundamental dimensions: mass, length, time, and temperature. After performing the dimensional analysis, there were four dimensionless groups for the peak net heat flux and six dimensionless groups for the total heating. Using the Chen method for dimensional analysis [33], the resulting dimensionless Π groups were determined. We assumed power law relationships between the Π group of interest and the remaining Π groups. After linearizing the equation, a linear regression was performed to determine the fit coefficients. Next, the linearized equation with the coefficients was converted back to the power law form which can be seen in Eqs. 4 and 5 for the peak net heat flux and total heating, respectively. In some cases it is useful to adjust Π groups to reflect the physical relationship between terms. For the dimensional analysis of Q, it was determined that t_c was an important parameter, but when t_c was initially included in the $q''_{net,peak}$ dimensional analysis, there was little correlation with t_c. This was not surprising since $q''_{net,peak}$ occurs at much shorter time scales than t_c. Therefore, t_c was not included in the final dimensional analysis for $q''_{net,peak}$.

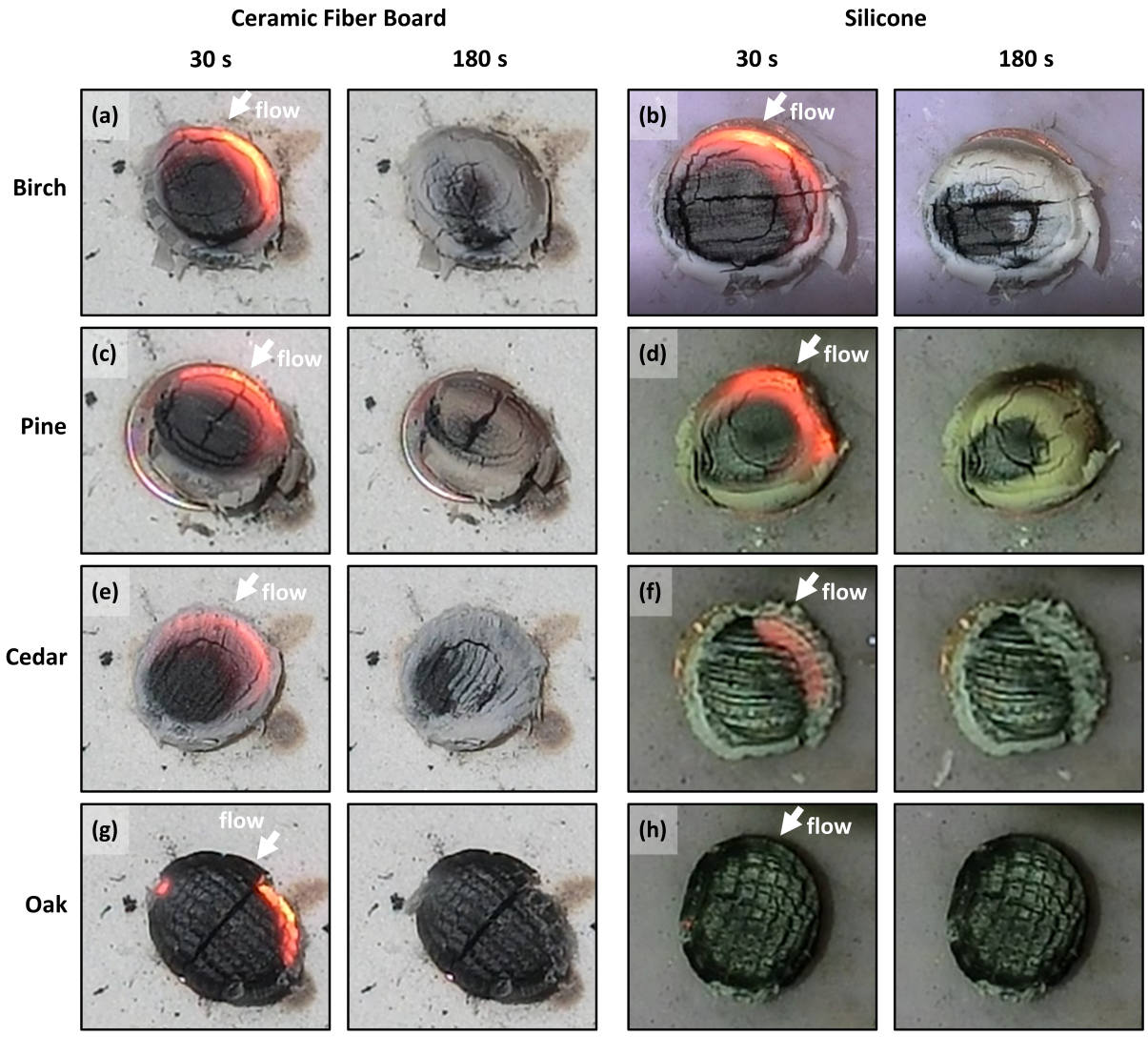

FIGURE 4: IMAGES SHOWING THE SMOLDERING PROGRESSION FOR THE 1 m/s FLOW CONDITION FOR SMALL FIREBRANDS OF FOUR WOOD TYPES ON CERAMIC FIBER BOARD AND SILICONE.

$$\frac{q''_{net,peak}\, r^3}{m\, U^3} = 3.35e8 \left(\frac{k_s\, T_{FB}\, r^2}{m\, U^3}\right)^{-0.466} \left(\frac{\rho_s\, r^3}{m}\right)^{0.457} \left(\frac{C_{p,s}\, T_{FB}}{U^2}\right)^{2.194} \quad (4)$$

$$\frac{Q\, t_c^2}{m} = 0.104 \left(\frac{k_s\, t_c^3\, T_{FB}}{m\, r}\right)^{0.291} \left(\frac{\rho_s\, r^3}{m}\right)^{-0.277} \left(\frac{C_{p,s}\, t_c^2\, T_{FB}}{r^2}\right)^{-0.151} \left(\frac{U\, t_c}{r}\right)^{-1.982} \left(\frac{q''_{net,peak,meas}\, t_c^3}{m}\right)^{0.554} \quad (5)$$

In Figures 9 and 10, the measured Π groups were compared to those predicted by Eqs. 4 and 5. Note that the $q''_{net,peak,meas}$ used in Eq. 5 was the measured value, not the calculated $q''_{net,peak}$ from Eq. 4. There was good agreement between the measured and predicted values for both the non-dimensional $q''_{net,peak}$ and the non-dimensional Q. The average difference between the measured and predicted was 19 % for $q''_{net,peak}$ and 13 % for Q. A possible limitation of applying this type of dimensional analysis is the risk of overfitting or collinearity of the parameters, which generates coefficients that are sensitive to small changes in the data set. As with any empirical correlation, the prediction cannot be expected to apply outside of the parameters used to generate the correlation, but these correlations provide some insight into the important factors for firebrand heat transfer, as discussed in the next section.

4.1 Discussion

The magnitude of the exponents on the dimensionless groups gave an indication of the relative importance of that parameter grouping. For instance, with $q''_{net,peak}$, the Π group with the substrate's heat capacity, $C_{p,s}$, had the largest exponent, meaning

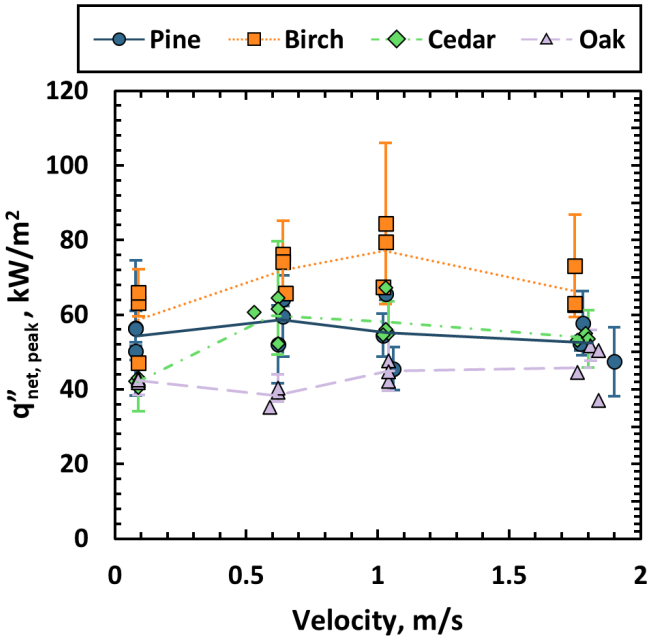

(a) Ceramic Fiber Board

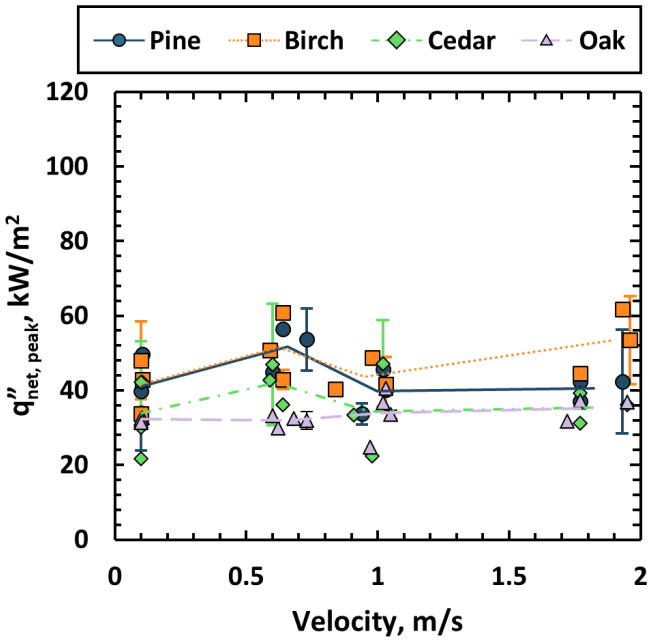

(b) Silicone

FIGURE 5: PEAK HEAT FLUX FOR SMALL FIREBRANDS OF ALL WOOD TYPES AND FLOW CONDITIONS (A) ON A CERAMIC FIBER BOARD SUBSTRATE AND (B) ON A SILICONE SUBSTRATE.

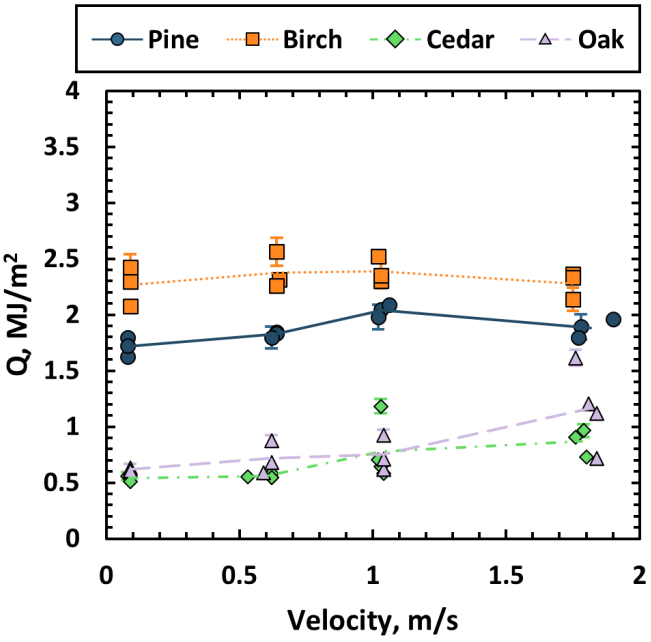

(a) Ceramic Fiber Board

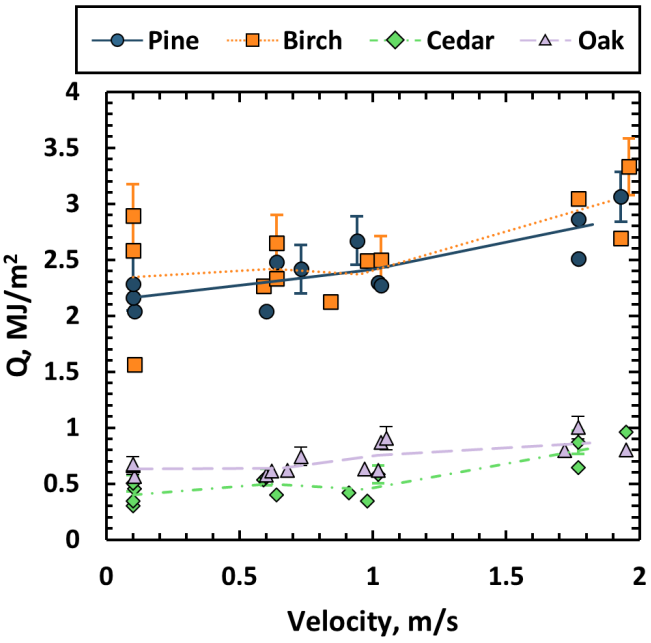

(b) Silicone

FIGURE 6: TOTAL HEATING FOR SMALL FIREBRANDS OF ALL WOOD TYPES AND FLOW CONDITIONS (A) ON A CERAMIC FIBER BOARD SUBSTRATE AND (B) ON A SILICONE SUBSTRATE.

this Π group was an important predictor of the peak net heat flux. Additionally, the Π groups in Eq. 4 containing the other substrate thermal properties, thermal conductivity and density, had nontrivial exponents, indicating their overall importance as well. In Figure 3, the substrate material appeared to have an effect on the heat flux profile. With the ceramic fiber board substrate, the q''_{stor} and $q''_{net,peak}$ were greater than the silicone substrate. However, the q''_{cond} increased faster for the silicone substrate, resulting in similar values for Q and t_c for both substrates. In Figures 5 and 6, we observed the trend that the ceramic fiber board experienced higher peak heat fluxes but similar total heating compared to the silicone substrate across all wood types. Pine was

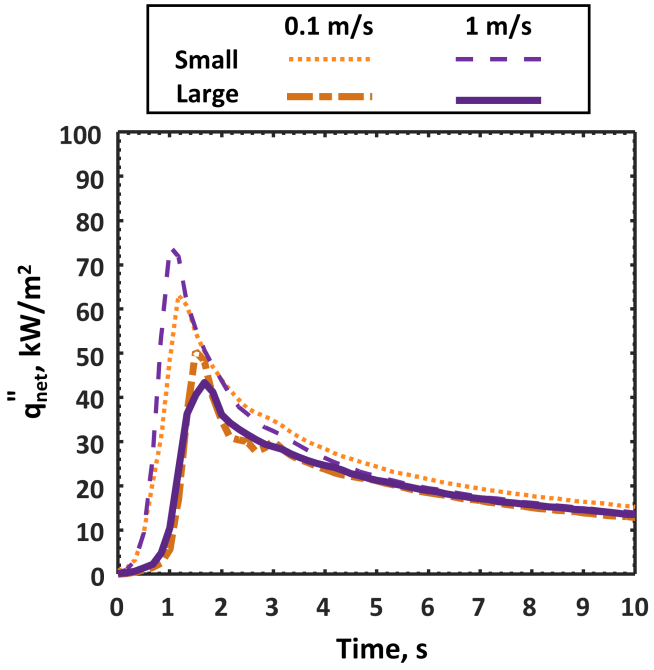

(a) Birch

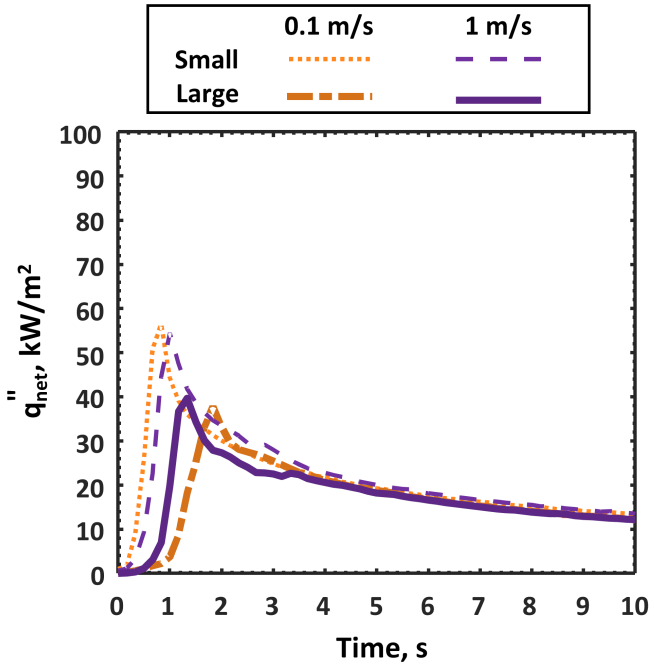

(b) Pine

FIGURE 7: REPRESENTATIVE NET HEAT FLUX PROFILES FOR BOTH SIZES OF (A) BIRCH FIREBRANDS AND (B) PINE FIREBRANDS TWO FLOW CONDITIONS.

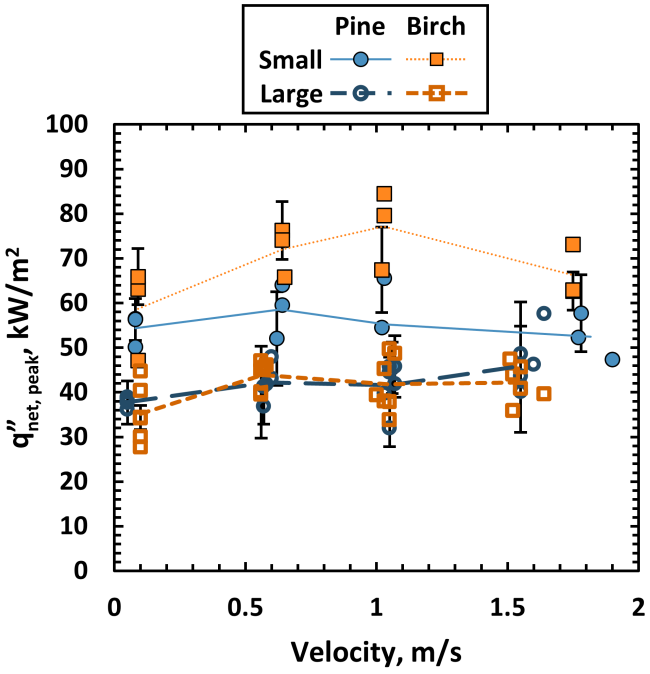

(a) Peak Heat Flux

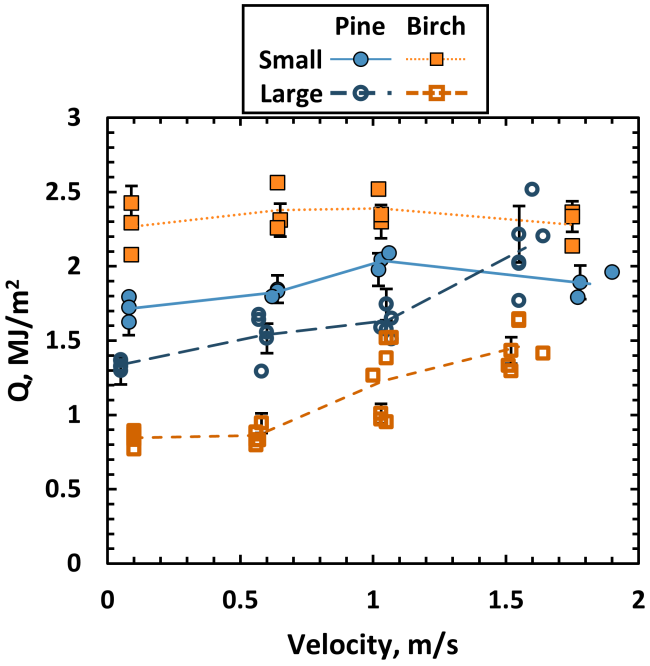

(b) Total Heating

FIGURE 8: THE (A) PEAK NET HEAT FLUX AND (B) TOTAL HEATING FOR BOTH SIZES OF PINE AND BIRCH FIREBRANDS ON THE CERAMIC FIBER BOARD SUBSTRATE AT ALL FOUR FLOW CONDITIONS.

the only wood type where the total heating changed slightly with substrate material, increasing for silicone compared to ceramic fiber board.

The weak impact of flow velocity on $q''_{net,peak}$ was also reinforced through the power law dependency in Eq. 4. Although U appeared in multiple dimensionless groups, the overall exponents of U are nearly identical on both sides of the equation, indicating a weak dependence on the flow condition. This was also evident in the experimental results. Referring back to Figures 5, 6, and 8, there was not a strong trend in $q''_{net,peak}$ or Q with flow condition. This finding was also observed for individual firebrands in several other studies [18, 23, 28]. The peak heat flux occurs within a few seconds. This likely means that the air flow condition does not

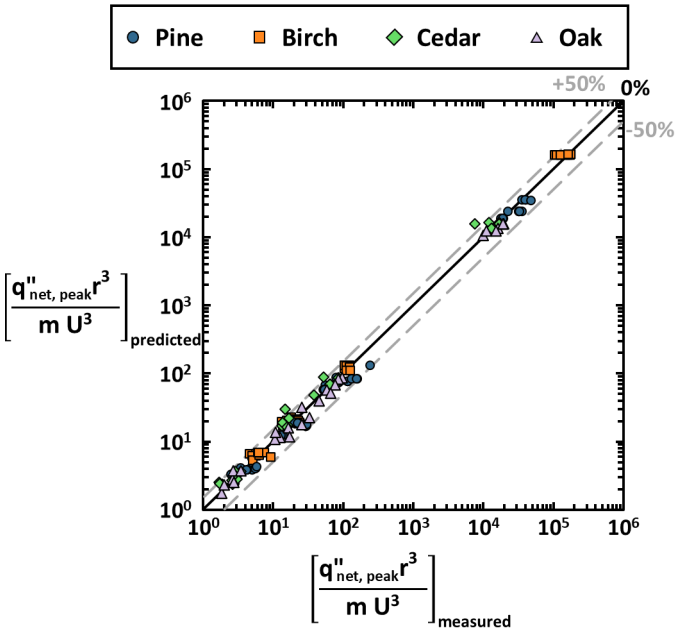

FIGURE 9: MEASURED NON-DIMENSIONAL PEAK NET HEAT FLUX VERSUS PREDICTED VALUES USING THE RELATIONSHIP IN EQ. 4.

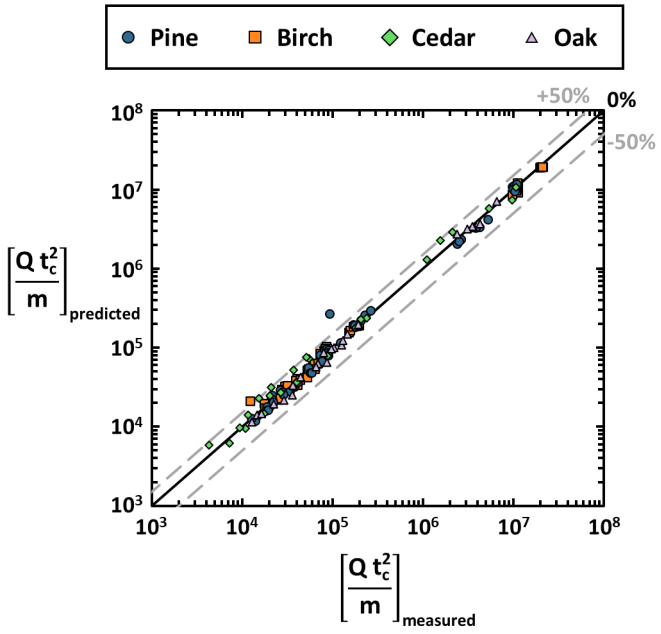

FIGURE 10: MEASURED NON-DIMENSIONAL TOTAL HEATING VERSUS PREDICTED VALUES USING THE RELATIONSHIP IN EQ. 5.

have enough time to act on the firebrand and influence the peak net heat flux values.

The dimensional analysis also reinforced the dependencies of $q''_{net,peak}$ and Q on the parameters representing wood type. In Eq. 4 for $q''_{net,peak}$, the two dimensionless Π groups containing T_{FB} both have significant exponents. In Eq. 5 for Q, in addition to T_{FB} there are two other parameters representing wood type, the $q''_{net,peak,meas}$ and t_c. The dimensionless Π group containing $q''_{net,peak,meas}$ appears important to Q, as this term had the second greatest exponent in Eq. 5. T_{FB} and t_c ended up in multiple dimensionless groups in Eq. 5, without significant overall exponents for either parameter. However, performing the dimensional analysis for Q without t_c would result in an overall error more than three times higher. This result supports the necessity of the combustion time parameter in predicting the total heating, which makes sense as Q is a time dependent integrated value.

The effects of firebrand radius were obscured in the dimensional analysis, as radius was one of the repeated variables. However, combining the exponents for r in Eq. 4 would result in an expected relationship of $q''_{net,peak} \propto r^{-2.6}$. Our experimental results in Figures 8a and 8b also showed that firebrand size (with disc aspect ratio held constant) had an effect on $q''_{net,peak}$ and the Q. The smaller radius firebrands generally experienced higher $q''_{net,peak}$ and Q when the wood type, flow condition, and substrate material were held constant. The trend was most distinct with the birch firebrands.

The differences in $q''_{net,peak}$ and Q with firebrand radius were possibly due to the differences in surface area and volume. The surface area of the large firebrand disc was approximately 1.8 times greater than the small firebrand disc. Assuming the convective heat transfer coefficients and firebrand temperatures were not affected by firebrand size, the large firebrands would experience more conductive, radiative, and convective cooling because of their larger surface area. Although the larger firebrands also had a larger area for smoldering reactions to take place, the smoldering/glowing reactions were localized to the leading edge of the firebrand, based on visual observations (refer to Fig. 4). The potential increase in smoldering heat generation did not appear to be enough to overcome the increased cooling from the larger surface area. Although researchers often treat firebrands as thermally lumped, as observed visually, there were clear differences in the surface temperature of the firebrand (Fig. 4). There were glowing areas on the top surface of the firebrand that were much hotter than the black areas of the surface. The firebrands were also thermally quenched on the bottom surface when they first contact the TSC. The larger firebrands were 1.3 times thicker than the small firebrands, meaning the hottest temperatures from the reacting surfaces at the top and leading edge had to conduct farther to heat up the TSC, allowing additional heat loss to the environment. Over most of the conditions, the greater surface area and thickness of the large firebrands led to lower $q''_{net,peak}$ and Q values compared to the small firebrands. Given the potential importance of surface area, this parameter could be used in future analysis to consider other types of firebrand geometries, such as longer cylinders or cuboids.

An additional consideration when looking at other firebrand shapes or larger sizes is non-uniformities in firebrand heating as was shown in localized heat flux measurements in Bearinger et al. [23]. Consequently, further study is necessary to determine the usefulness or limitations of Eqs. 4 and 5 for larger firebrands and different geometries. Overall, with additional work, these and other parameters could be used for ignition prediction correlations, such as for ignition time in Zhu and Urban [26].

5. CONCLUSIONS

The peak net heat flux and total heating from individual firebrand discs of four different wood types and two sizes were measured using a TSC with a ceramic fiber board substrate and with a silicone substrate under four air flow conditions. Across all experiments, the peak net heat flux occurred within the first few seconds and ranged between 22 kW/m^2 and 84 kW/m^2. The parameter with the clearest impact on the peak net heat flux was the size of the firebrand. The small firebrands experienced higher peak net heat flux values than the large firebrands when other parameters were held constant. The total heating varied between 0.3 MJ/m^2 and 3.3 MJ/m^2 for the different wood types, firebrand sizes, substrate materials, and flow conditions. There were clear differences in the total heating due to the size of the firebrand, with the smaller firebrands generating higher total heating values, which is attributed to the smaller firebrands having a smaller surface area for heat losses. The total heating from large pine and birch firebrands showed an increase with flow velocity, but there was not a clear trend in the peak net heat flux with flow condition. Future work could investigate the substrate and size effects of more wood types and if wood properties could be used to explain any of the trends observed.

From the data, two correlations were determined using dimensional analysis to predict the peak net heat flux and total heating measured in the laboratory. The peak net heat flux from the correlation was on average 19 % different from the measured values. The average difference for the total heating was much lower at 13 %. The correlations showed that the heat transfer from the firebrands was strongly dependent upon the substrate thermal properties and nearly independent of the air flow condition. Although caution should be taken before applying the correlations outside the laboratory, the general dependencies can inform efforts to model the complicated firebrand ignition process with simpler parameters and enable fire modeling to inform the design of more fire-resistant structures and communities.

ACKNOWLEDGMENTS

The authors would like to thank Jae Hyun Kim of the NIST Heat Transfer and Alternative Energy Systems Group for completing thermal conductivity measurements of the silicone material.

REFERENCES

[1] Parks, S. A. and Abatzoglou, J. T. "Warmer and Drier Fire Seasons Contribute to Increases in Area Burned at High Severity in Western US Forests From 1985 to 2017." *Geophysical Research Letters* Vol. 47 No. 22 (2020). DOI 10.1029/2020GL089858.

[2] Radeloff, V.C., Helmers, D.P., Kramer, H.A., Mockrin, M.H., Alexandre, P.M., Bar-Massada, A., Butsic, V., Hawbaker, T.J., Martinuzzi, S., Syphard, A.D. and Stewart, S.I. "Rapid growth of the US wildland-urban interface raises wildfire risk." *Proceedings of the National Academy of Science* Vol. 115(13) (12 March 2018): pp. 3314– 3319. DOI 10.1073/pnas.1718850115.

[3] Maranghides, Alexander, Link, Eric, Mell, William "Ruddy", Hawks, Steven, Wilson, Mike, Brewer, Will, Brown, Chris, Vihnaneck, Bob and Walton, William D. "A Case Study of the Camp Fire – Fire Progression Timeline." *NIST Technical Note TN 2135, National Institute of Standards and Technology, Gaithersburg, MD* (Jan 2021)DOI 10.6028/NIST.TN.2135.

[4] Rains, Molly. "Maui's deadly blazes reveal a fire-prone Hawaii." *Science* Vol. 381 No. 6659 (2023): pp. 718–719.

[5] Nazare, Shonali, Leventon, Isaac and Davis, Rick. "Ignitibility of Structural Wood Products Exposed to Embers During Wildland Fires: A Review of Literature." *NIST Technical Note TN 2153, National Institute of Standards and Technology, Gaithersburg, MD* (April 2021)DOI 10.6028/NIST.TN.2153.

[6] Blanchi, Raphaele and Leonard, Justin. "Investigation of bushfire attack mechanisms resulting in house loss in the ACT bushfire 2003." *Bushfire CRC report* (2005).

[7] Graham, Russell, Finney, Mark, McHugh, Chuck, Cohen, Jack, Calkin, Dave, Stratton, Rick, Bradshaw, Larry and Nikolov, Ned. *Fourmile Canyon Fire Findings* (2012). DOI 10.2737/rmrs-gtr-289.

[8] Maranghides, Alexander and Mell, William E. "A Case Study of a Community Affected by the Witch and Guejito Fires." *NIST Technical Note TN 1635, National Institute of Standards and Technology, Gaithersburg, MD* (2009)DOI 10.6028/NIST.TN.1635.

[9] Ribeiro, Luís M., Rodrigues, André, Lucas, Davi and Viegas, Domingos Xavier. "The Impact on Structures of the Pedrógão Grande Fire Complex in June 2017 (Portugal)." *Fire* Vol. 3 No. 4 (2020). DOI 10.3390/fire3040057.

[10] Manzello, Samuel L., Cleary, Thomas G., Shields, John R. and Yang, Jiann C. "On the ignition of fuel beds by firebrands." *Fire and Materials* Vol. 30 No. 1 (2006): pp. 77–87. DOI 10.1002/fam.901.

[11] Urban, James L., Song, Jiayun, Santamaria, Simon and Fernandez-Pello, Carlos. "Ignition of a spot smolder in a moist fuel bed by a firebrand." *Fire Safety Journal* Vol. 108 (2019): p. 102833. DOI 10.1016/j.firesaf.2019.102833. Accessed 2024-09-16, URL https://linkinghub.elsevier.com/retrieve/pii/S0379711218304168.

[12] Wessies, Savannah S, Chang, Michael K, Marr, Kevin C and Ezekoye, Ofodike A. "Experimental and analytical characterization of firebrand ignition of home insulation materials." *Fire Technology* Vol. 55 (2019): pp. 1027–1056. DOI 10.1007/s10694-019-00818-8.

[13] Yang, Guang, Ning, Jibin, Shu, Lifu, Zhang, Jili, Yu, Hongzhou and Di, Xueying. "Spotting ignition of larch (Larix gmelinii) fuel bed by different firebrands." *Journal of Forestry Research* Vol. 33 No. 1 (2022): pp. 171–181. DOI 10.1007/s11676-020-01282-9. Accessed 2024-09-16, URL https://link.springer.com/10.1007/s11676-020-01282-9.

[14] Manzello, Samuel L., Suzuki, Sayaka, Gollner, Michael J. and Fernandez-Pello, A. Carlos. "Role of firebrand combustion in large outdoor fire spread." *Progress in Energy and Combustion Science* Vol. 76 (2020): p. 100801. DOI https://doi.org/10.1016/j.pecs.2019.100801. URL https://www.sciencedirect.com/science/article/pii/S0360128519300942.

[15] Rein, Guillermo. "Smoldering combustion." *SFPE Handbook of Fire Protection Engineering*. Springer (2016): pp. 581–603.

[16] Babrauskas, Vytenis. "Ignition Handbook." *Fire Science Publishers, Issaquah, WA* (2014).

[17] Ohlemiller, Thomas J. and Villa, Kate M. "Material Flammability Test Assessment for Space Station Freedom." *NIST Internal Report IR 4591, National Institute of Standards and Technology, Gaithersburg, MD* (June 1991)DOI 10.6028/NIST.IR.4591.

[18] Hakes, Raquel S.P., Salehizadeh, Hamed, Weston-Dawkes, Matthew J. and Gollner, Michael J. "Thermal characterization of firebrand piles." *Fire Safety Journal* Vol. 104 (2019): pp. 34–42. DOI 10.1016/j.firesaf.2018.10.002.

[19] Tao, Zhenxiang, Bathras, Bryce, Kwon, Byoungchul, Biallas, Ben, Gollner, Michael J. and Yang, Rui. "Effect of firebrand size and geometry on heating from a smoldering pile under wind." *Fire Safety Journal* Vol. 120 (2021): p. 103031. DOI 10.1016/j.firesaf.2020.103031. Fire Safety Science: Proceedings of the 13th International Symposium.

[20] Thomas, J. Christian, Mueller, Eric V. and Hadden, Rory M. "Estimating net heat flux from surrogate firebrand accumulations using an inverse heat transfer approach." *Advances in Forest Fire Research 2018 - D. X. Viegas (Ed.)* (November 2018): p. 769DOI 10.14195/978-989-26-16-506_84.

[21] Salehizadeh, Hamed, Hakes, Raquel S. P. and Gollner, Michael J. "Critical Ignition Conditions of Wood by Cylindrical Firebrands." *Frontiers in Mechanical Engineering* Vol. 7 (2021): p. 630324. DOI 10.3389/fmech.2021.630324.

[22] Richter, Franz, Bathras, Bryce, Barbetta Duarte, Julia and Gollner, Michael J. "The Propensity of Wooden Crevices to Smoldering Ignition by Firebrands." *Fire Technology* (2022): pp. 1–22DOI 10.1007/s10694-022-01247-w.

[23] Bearinger, Elias D, Hodges, Jonathan L, Yang, Fengchang, Rippe, Christian M and Lattimer, Brian Y. "Localized heat transfer from firebrands to surfaces." *Fire Safety Journal* Vol. 120 (2021): p. 103037. DOI 10.1016/j.firesaf.2020.103037.

[24] Mensch, Amy E., Wessies, Savannah S., Hamins, Anthony and Yang, Jiann C. "Measuring firebrand heat flux with a thin-skin calorimeter." *Fire Safety Journal* Vol. 140 (2023): p. 103859. DOI 10.1016/j.firesaf.2023.103859.

[25] De Beer, Jacques A., Dietz, Emily L., Stoliarov, Stanislav I. and Gollner, Michael J. "An empirical firebrand pile heat flux model." *Fire Safety Journal* Vol. 141 (2023): p. 104004. DOI 10.1016/j.firesaf.2023.104004. Accessed 2025-11-17, URL https://linkinghub.elsevier.com/retrieve/pii/S0379711223002722.

[26] Zhu, Luqing and Urban, James L. "Analyzing the ignition capabilities of glowing firebrand accumulations." *Proceedings of the Combustion Institute* Vol. 40 No. 1 (2024): p. 105746. DOI https://doi.org/10.1016/j.proci.2024.105746. URL https://www.sciencedirect.com/science/article/pii/S1540748924005546.

[27] Suzuki, Sayaka and Manzello, Samuel L. "Experimental investigation of firebrand accumulation zones in front of obstacles." *Fire Safety Journal* Vol. 94 (2017): pp. 1–7. DOI 10.1016/j.firesaf.2017.08.007. Accessed 2025-11-17, URL https://linkinghub.elsevier.com/retrieve/pii/S0379711217303326.

[28] Wong, Steven, Hodges, Jonathan L. and Lattimer, Brian Y. "Impact of ash layer retention on heat transfer in piles of vegetation and structure firebrands." *Fire Safety Journal* Vol. 134 (2022): p. 103694. DOI 10.1016/j.firesaf.2022.103694. Accessed 2024-12-12, URL https://linkinghub.elsevier.com/retrieve/pii/S0379711222001710.

[29] Bearinger, Elias, Lattimer, Brian Y., Hodges, Jonathan L., Rippe, Christian and Kapahi, Anil. "Statistical Assessment of Parameters Affecting Firebrand Pile Heat Transfer to Surfaces." *Frontiers in Mechanical Engineering* Vol. 7 (2021): p. 702181. DOI 10.3389/fmech.2021.702181. Accessed 2024-12-11, URL https://www.frontiersin.org/articles/10.3389/fmech.2021.702181/full.

[30] Incropera, Frank P. and DeWitt, David P. *Fundamentals of Heat and Mass Transfer*, 5th ed. John Wiley Sons, Inc., New York City, New York (2002).

[31] ASTM Committee E21. "Standard Test Method for Measuring Heat Transfer Rate Using a Thin-Skin Calorimeter." (2016). DOI 10.1520/E0459-05R16. Accessed 2022-10-04, URL http://www.astm.org/cgi-bin/resolver.cgi?E459-05R16.

[32] Hidalgo, Juan P, Maluk, Cristian, Cowlard, Adam, Abecassis-Empis, Cecilia, Krajcovic, Michal and Torero, José L. "A Thin Skin Calorimeter (TSC) for quantifying irradiation during large-scale fire testing." *International Journal of Thermal Sciences* Vol. 112 (2017): pp. 383–394. DOI 10.1016/j.ijthermalsci.2016.10.013.

[33] Chen, JJJ. "An improvement on the quraishi-fahidy method of dimensional analysis." *The Canadian Journal of Chemical Engineering* Vol. 66 No. 4 (1988): pp. 701–702. DOI 10.1002/cjce.5450660428.